



OPEN

Stability of hypothetical $\text{Ag}^{\text{II}}\text{Cl}_2$ polymorphs under high pressure, revisited: a computational study

Adam Grzelak[✉] & Wojciech Grochala

A comparative computational study of stability of candidate structures for an as-yet unknown silver dichloride AgCl_2 is presented. It is found that all considered candidates have a negative enthalpy of formation, but are unstable towards charge transfer and decomposition into silver(I) chloride and chlorine within the DFT and hybrid-DFT approaches in the entire studied pressure range. Within SCAN approach, several of the “true” $\text{Ag}^{\text{II}}\text{Cl}_2$ polymorphs (i.e. containing Ag(II) species) exhibit a region of stability below ca. 20 GPa. However, their stability with respect to aforementioned decomposition decreases with pressure by account of all three DFT methods, which suggests a limited possibility of high-pressure synthesis of AgCl_2 . Some common patterns in pressure-induced structural transitions observed in the studied systems also emerge, which further testify to an instability of hypothetical AgCl_2 towards charge transfer and phase separation.

Chemistry of silver(II) compounds constitutes a topic of studies that is both demanding—particularly due to the extremely strong oxidizing properties of these compounds—as well as interesting, as evidenced by the body of works discussing them in relation to oxocuprates—a well-known family of precursors for high-pressure superconductors^{1,2}. Inspired by experimental works exploring high-pressure phase transitions of AgF_2 ^{3,4}, as well as most recent computational study of thermodynamic stability of hypothetical mixed-valence silver fluorides (including at elevated pressure conditions)⁵, this work is a continuation to a previous systematic study, which explored relative stability of multiple hypothetical polymorphs of $\text{Ag}^{\text{II}}\text{Cl}_2$ —an as-yet unknown analogue of AgF_2 ⁶. The aforementioned study found that a true silver(II) chloride is likely to be unstable towards charge transfer and phase separation into AgCl and Cl_2 at ambient pressure conditions. This work aims to extend these considerations into high-pressure regime, in the hope that applying extreme conditions could stabilize $\text{Ag}^{\text{II}}\text{Cl}_2$. In particular, the previous study found that a layered, AgF_2 -type polymorph of AgCl_2 could be stabilized at a pressure of ca. 35 GPa, due to relatively low molar volume⁶.

The interest in this particular compound stems from its potential similarity to AgF_2 , which has recently been shown to be an excellent analog of oxocuprates in terms of structure and very strong magnetic interactions². In fact, $\text{Ag}^{\text{II}}\text{Cl}_2$ —if obtained, and providing a suitable structural arrangement—could be expected to host even stronger antiferromagnetic superexchange than AgF_2 , due to stronger covalence of Ag–Cl bonding, as predicted from differences in electronegativity (Ag: 1.93, Cl: 3.16, F: 3.98—Pauling scale). Overall, this work is part of a joint computational and experimental effort: to synthesize $\text{Ag}^{\text{II}}\text{Cl}_2$ utilizing high pressure and high temperature experimental techniques, coupled with computational methods providing insight into understanding the expected products and phases. On top of that, the added value of studies in high-pressure regime is that the observed changes in structure and bonding induced by pressure can provide meaningful insight into the chemical nature of the studied compounds⁷.

Results

Stability of AgCl_2 phases. Seven different candidate structures for polymorphs of AgCl_2 were considered in this work. Six of them were derived from the previous, ambient-pressure study⁶. They were:

- AgF_2 type (*Pbca*)—corrugated layers made up of $[\text{AgCl}_4]$ square subunits;
- CuCl_2 type (*P1*)—1D chains made up of $[\text{AgCl}_4]$ square subunits;
- AuCl_2 type (*P-1*)—a kind of nanotubular polymorph derived from 0D molecular structure of AuCl_2 (see below);
- $\text{Ag}(\text{I})\text{r}$ type (*P-1*)—a structure composed of double layers of rocksalt-type AgCl interspersed with Cl_2 bridges;

Center for New Technologies, University of Warsaw, Banacha 2C, 02-097 Warszawa, Poland. ✉ email: a.grzelak@cent.uw.edu.pl

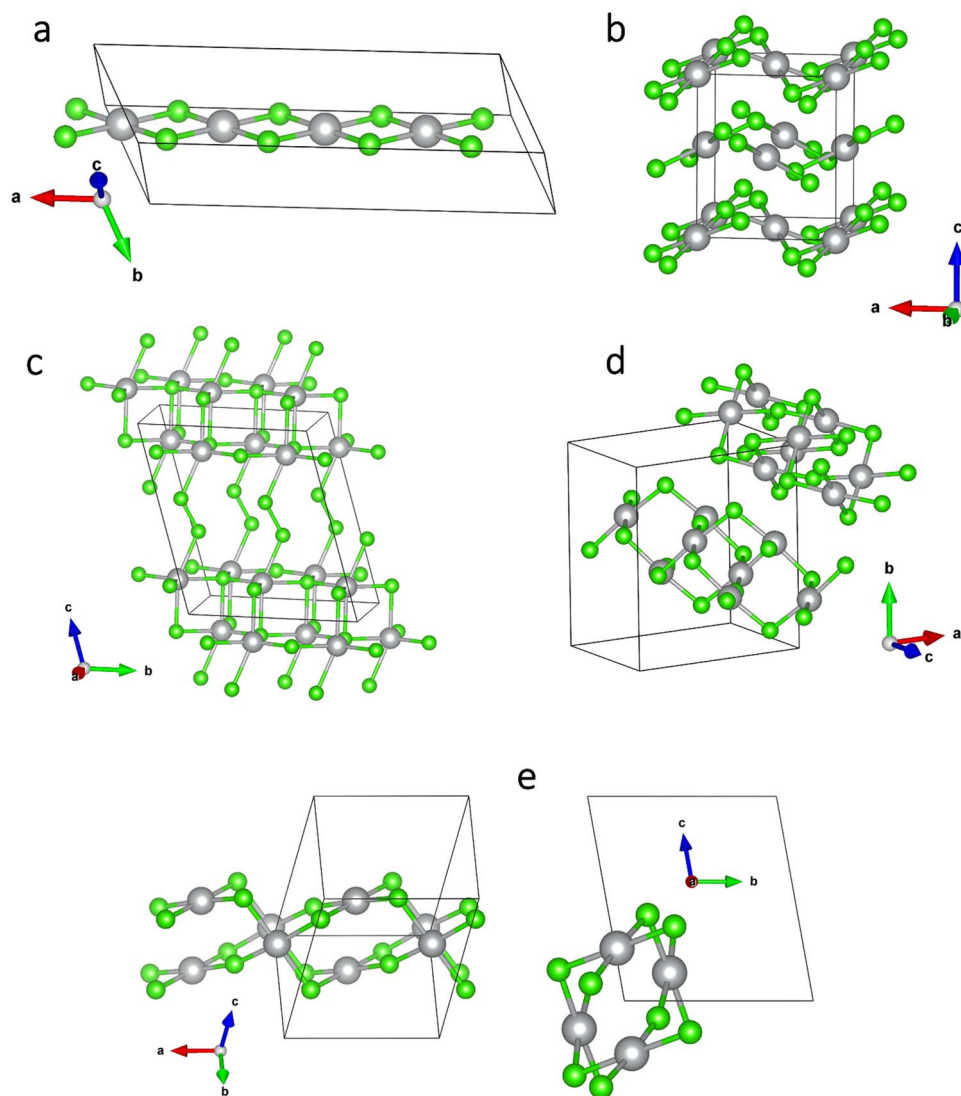


Figure 1. Selected structures of AgCl_2 candidate polymorphs. (a) CuCl_2 -type, (b) AgF_2 -type, (c) Ag(I)r , (d) AgF_2 -HP-type, (e) AuCl_2 -type. Ag—grey, Cl—green.

- Ag(I)h type ($P-1$)—similar as above, but with hexagonal double layers of AgCl ;
- MnO_2 type ($P2_1/c$)—a different arrangement of corrugated layers made up of pairs of $[\text{AgCl}_4]$ square subunits.

Additionally, the high-pressure, nanotubular polymorph of AgF_2 (referred to as HP- AgF_2 , space group $Pbcn$) was considered as a candidate⁴. Structures of selected polymorphs described above are presented in Fig. 1. Structures of all of the aforementioned candidate polymorphs are provided in Supplementary Information.

Importantly, Ag(I)r and Ag(I)h polymorphs do not contain Ag(II) species and instead are composed of sub-structures of $\text{Ag}^{\text{I}}\text{Cl}$ and Cl_2 molecules. For the remaining five $\text{Ag}^{\text{I}}\text{Cl}_2$ polymorphs containing paramagnetic d^9 silver cation, magnetic interactions were taken into account:

- AgF_2 type: 2D antiferromagnetic (AFM) coupling within layers;
- CuCl_2 type: AABB-type AFM coupling within chains, known to exist in CuCl_2 ⁸, and found to be the lowest-energy magnetic solution for AgCl_2 in this arrangement⁶;
- AgF_2 HP type: magnetic dimers coupled along ~ 180 degrees Ag-F-Ag bridges within nanotubes;
- MnO_2 type: AABB-type AFM coupling—ferromagnetic (FM) between adjacent $[\text{AgCl}_4]$ squares and AFM between pairs.

The AuCl_2 type derives from a structure of gold(I,III) chloride, a mixed-valence compound which consists of Au_4Cl_8 molecules, each containing two Ag(I) and two Ag(III) species⁹. When this structure is taken as a starting point for geometry optimization, all three computational methods yield a nanotubular polymorph somewhat

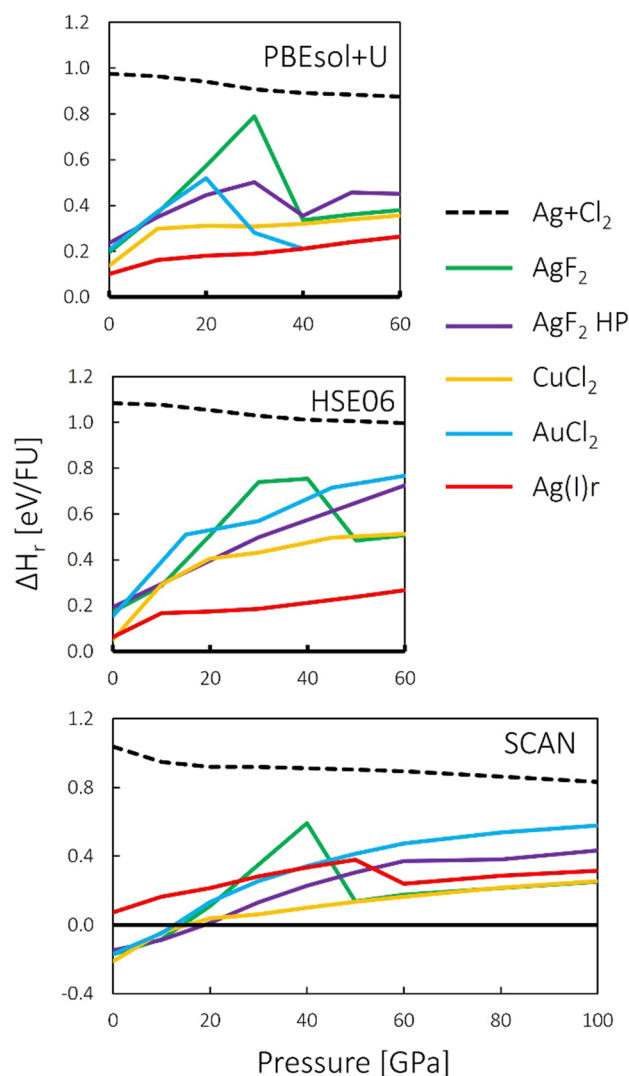


Figure 2. Stability of selected studied polymorphs of AgCl_2 , plotted as enthalpy per formula unit relative to $\text{AgCl} + \frac{1}{2}\text{Cl}_2$ (ΔH_r). Top panel—PBEsol+U (GGA functional), middle panel—HSE06 (hybrid functional), bottom panel—SCAN (meta-GGA functional). *FU* formula unit.

similar to the AgF_2 HP type. However, only the HSE06 approach is able to reproduce the mixed-valence nature of AuCl_2 and of the corresponding nanotubular polymorph of AgCl_2 derived from the former (as evidenced by two different coordination patterns of Ag sites in that solution)⁶. On the other hand, in the PBEsol+U and SCAN calculations, a magnetic model with dimers as in the AgF_2 HP type polymorphs was considered.

Stability of the studied candidate structures was evaluated using two parameters: (a) enthalpy of formation (labelled henceforth as ΔH_f), according to a reaction:



and (b) stability towards decomposition into AgCl and Cl_2 (ΔH_r), or more precisely, the enthalpy of reaction:



Defined in this manner, both parameters indicate thermodynamic instability when positive. Figure 2 shows plots of stability of studied AgCl_2 candidate types in terms of ΔH_r for all three methods used in this work. Enthalpy of $\text{Ag} + \text{Cl}_2$ mixture relative to $\text{AgCl} + \frac{1}{2}\text{Cl}_2$ is also plotted for comparison.

The studied polymorphs exhibit negative (favorable) enthalpies of formation within the entire studied pressure range in all three computational approaches. This is indirectly visible in Fig. 2 as the fact that curves for those polymorphs lie below the curve for $\text{Ag} + \text{Cl}_2$. On the other hand, they were found to be unstable in terms of ΔH_r in the entire studied pressure range within PBEsol+U and HSE06. However, results of SCAN calculations indicate moderate stability of $\text{Ag}^{\text{II}}\text{Cl}_2$ polymorphs below ca. 20 GPa. $\text{Ag}(\text{I})\text{r}$ polymorph is the most stable

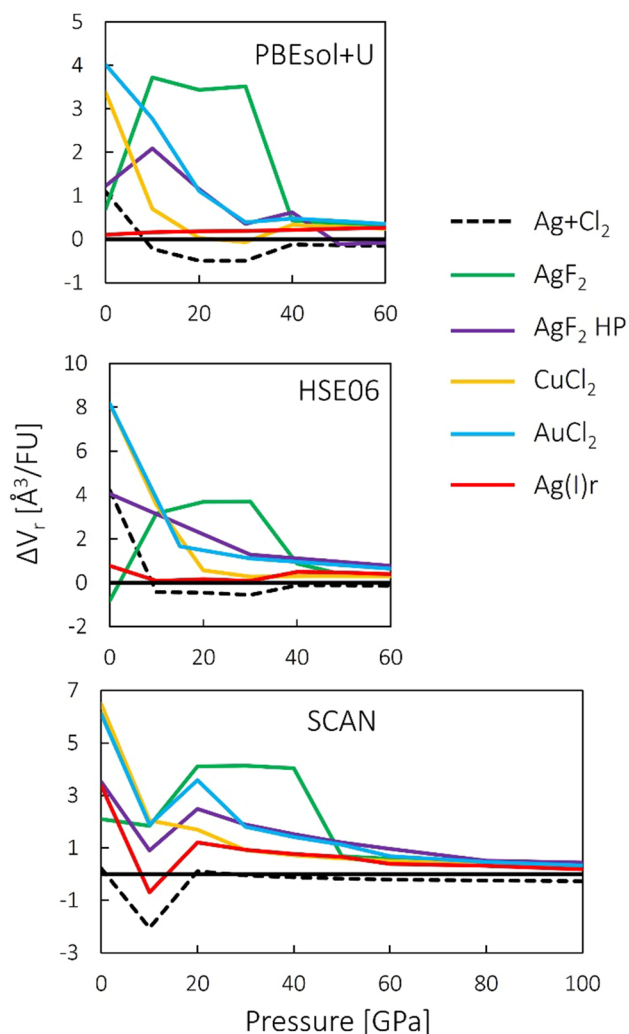


Figure 3. Volume of selected studied polymorphs of AgCl_2 relative to $\text{AgCl} + \frac{1}{2}\text{Cl}_2$. Top panel—PBEsol + U, middle panel—HSE06 (hybrid functional), bottom panel—SCAN (meta-GGA functional). *FU* formula unit.

among AgCl_2 candidate structures, according to PBEsol + U and HSE06 results, while this is not the case in SCAN picture. Given that it contains separate sub-phases of AgCl and Cl_2 , this further points to an instability towards charge transfer and phase separation.

The initial set of calculations was performed within the PBEsol + U approach, as the least computationally demanding. It was found that the Ag(I)h type collapses upon compression to 10 GPa into the Ag(I)r structure and it was not considered any further in the analogous HSE06 and SCAN calculations. Similarly, MnO_2 type was also neglected past the PBEsol + U approach, as it was found to be the least stable in terms of ΔH_f among the studied types. Therefore, these two polymorphs are not taken into account in Figs. 1, 2 and 3.

Figure 3 compares relative volume (ΔV_r) of the studied polymorphs with respect to $\text{AgCl} + \frac{1}{2}\text{Cl}_2$ mixture. Since the pV term becomes a considerable contribution to enthalpy at elevated pressures, the fact that most of the candidates for AgCl_2 considered here have a positive ΔV_r can be seen as an important factor leading to their relative instability. However, it should be noted that only HSE06 accurately reproduces ambient-pressure volumes of AgCl and Cl_2 . PBEsol + U underestimates the volume of AgCl and Cl_2 , while SCAN—that of Cl_2 . Therefore, ΔV_r values at 0 GPa in Fig. 3, and by extension—initial compressibilities—should be taken with a grain of salt. A noticeable dip at 10 GPa within the SCAN approach is likely a manifestation of this. The computationally demanding HSE06 results are likely to be the most correct.

Some of the features in Figs. 2 and 3, such as abrupt changes of relative energies or volumes, and apparent convergence of plots corresponding to different polymorphs are indicative of structural transitions. The nature and implication of those transition will be discussed in the next section.

Pressure-induced structural transitions. As an introduction to analysis of structural transitions of AgCl_2 polymorphs, let us first discuss the Ag(I)r solution. As mentioned before, this structure is made up of subunits of rocksalt-type AgCl and of Cl_2 molecules. Within the studied pressure range, it undergoes structural

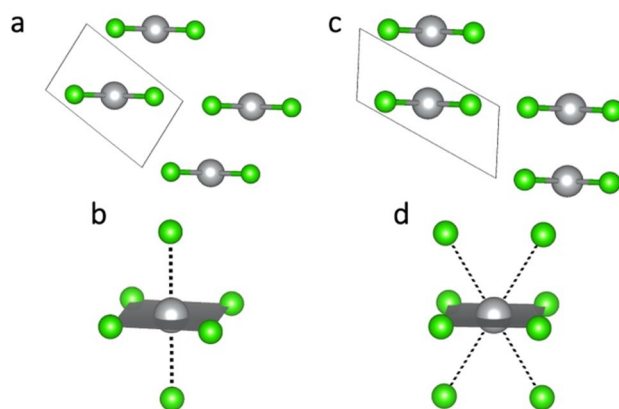


Figure 4. Structural changes in CuCl₂-polymorph. (a,c) View along the direction of chain propagation at 10 and 20 GPa, respectively. (b,d) View of local coordination of Ag at 10 and 20 GPa, respectively. Ag—grey, Cl—green.

rearrangements, which can be approximated as a sequence of deformations of the AgCl double layers, leading from a fundamentally NaCl-like coordination patterns to CsCl-like patterns, with increasing coordination number of Ag atoms. Importantly, it should be stressed again that this structure emerged as one of the lowest-energy solutions in an evolutionary algorithm structural search reported in the previous contribution⁶. It should not be treated as a viable candidate for the structure of AgCl₂, but rather as a manifestation of the proclivity of the studied system towards charge transfer and phase separation. The case for instability of Ag^ICl₂ towards these processes is further strengthened by the fact that the Ag(I)r polymorph remains the most stable (with respect to ΔH_f) throughout the studied pressure range in both PBESol + U and HSE06 approaches. A noticeable drop in ΔH_f between 50 and 60 GPa for this polymorph in the SCAN approach was the reason for extending the studied pressure range to 100 GPa in this case. However, this drop is a result for NaCl–CsCl-like transition in the AgCl subphase, which is more abrupt than in analogous PBESol + U and HSE06 calculations. No further phase transitions for Ag(I)r polymorph are observed up to 100 GPa.

The CuCl₂-type polymorph emerges as the most structurally robust in this study, as it does not undergo any collapse or drastic deformation in the studied pressure range, maintaining a relatively low ΔV_f in all three methods. The only change to the structure of this polymorph occurs in terms of arrangement of chains relative to one another. Up to 10 GPa (in all three computational approaches), the chains are positioned as in Fig. 4a, resulting in octahedral coordination of Ag atoms (Fig. 4b). The octahedra are elongated by 29%, 29% and 25%, according to PBESol, HSE06 and SCAN, respectively. By account of all three methods, the arrangement changes between 10 and 20 GPa, leading to a 4 + 4 coordination of Ag atoms, with the 4 inter-chain contacts longer by 23 to 33%, depending on the method (Fig. 4d). This is achieved in different ways: in PBESol + U and HSE06 results, the chains move relative to one another in a direction perpendicular to direction of propagation (Fig. 4c). In SCAN approach, this is achieved through a change of one of the unit cell angles, which results in sliding the chains relative to each other. The resulting 4 + 4 coordination is the same in all cases (Fig. 4d), but the longer Cl contacts are aligned parallel (in SCAN) or perpendicular (in PBESol + U and HSE06) to direction of propagation. Further compression to 30 GPa transforms the structure into that seen at 20 GPa in PBESol + U and HSE06 pictures. All of these transitions can be seen as a means to achieve a more efficient packing of chains (as evidenced by increasing coordination number of Ag). Changes in local coordination of Ag atoms in this polymorph are plotted in the top panel of Fig. 6.

Another result of these rearrangements is a reduction of Cl...Cl distances between neighboring chains. These distances drop from ca. 3.8 to 2.7 Å between 0 and 60 GPa in HSE06, compared to 3.2 to 2.5 Å in PBESol + U and 3.5 to 2.8 Å in SCAN. Recall that only HSE06 correctly reproduced the ambient pressure (low-temperature) volume of solid molecular Cl₂ at 0 GPa, so these results testify to the superiority of HSE06 in describing weak interactions compared to the other two methods utilized here (and free from the explicit van der Waals terms). Importantly, all of these distances are larger than the Cl–Cl bond in solid molecular Cl₂, which remains at ca. 2.00 Å and contracts very little (less than 0.05 Å) with compression in results from all three methods. Additionally, this polymorph was further optimized at 100 GPa with PBESol + U and SCAN methods, and does not undergo any structural modifications in that pressure range.

AgF₂-type polymorph undergoes substantial structural rearrangements with increasing pressure. At 0 GPa, it adopts a layered structure of *Pbca* space group (Fig. 5a), in which every Ag atom forms 4 in-layer bonds with Cl atoms, with two additional Cl atoms from adjacent layers together constituting a distorted octahedral coordination (Fig. 5b). The axial Cl contacts are noticeably longer (by 23%, 33% and 27% in PBESol + U, HSE06 and SCAN, respectively) than equatorial ones. The same phenomenon is observed in AgF₂ and in general, elongated octahedral coordination is a well-documented phenomenon in silver(II) fluorides (which includes ternary compounds)¹⁰. This is usually attributed to Jahn–Teller effect, whereby a vibronic instability leads to elongation or contraction of bonds along one of the three axes of octahedron, which lowers the overall electronic energy. Upon compression, this elongation is reduced in AgCl₂ down to 1%–2% at 30 GPa in both PBESol + U and SCAN

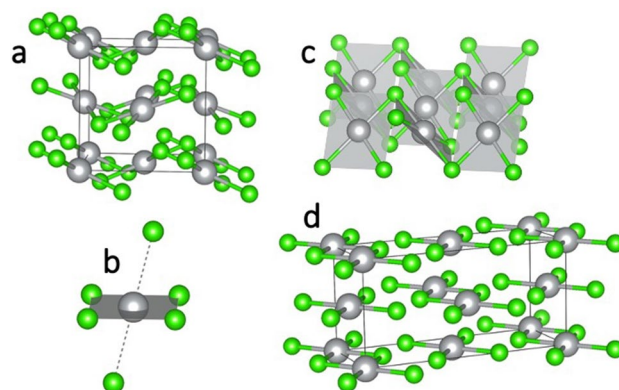


Figure 5. Structural features of AgF_2 -type polymorph: **(a)** ambient-pressure structure; **(b)** local coordination of Ag in the ambient-pressure structure; **(c)** one layer at 40 GPa in HSE06 approach—note that axial Cl atoms are now within the same layer, a pair of those contacts is marked with red dashed line; **(d)** structure resulting from phase transition between 40 and 50 GPa (30 and 40 GPa in PBEsol + U approach). Note the CuCl_2 -like chains. Ag—grey, Cl—green.

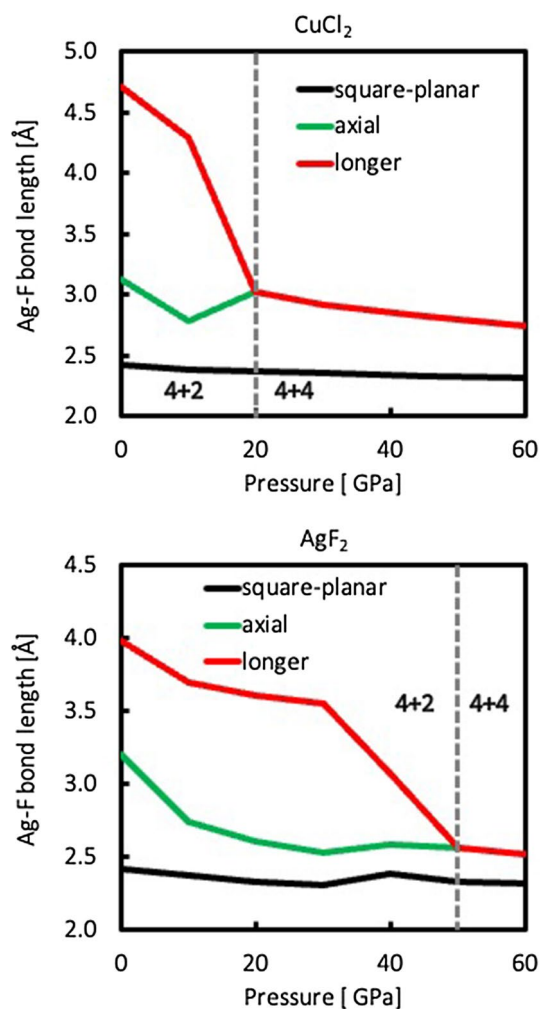


Figure 6. Pressure dependence of Ag-F distances in CuCl_2 -type and AgF_2 -type polymorphs in the HSE06 picture.

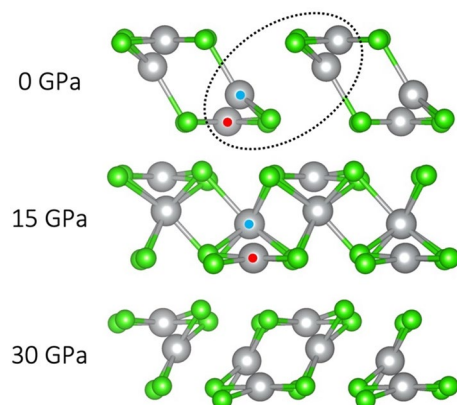


Figure 7. Structural transition of AuCl_2 -type polymorph in the HSE06 picture. Nanotubes are viewed along the axis of propagation. Blue and red circles indicate Ag(I) and Ag(III) species, respectively.

results. The structure at this point is reminiscent of high-pressure structure of PdF_2 ¹¹, which—like AgF_2 —can be described as a distorted fluorite, but lacks Jahn–Teller elongation of $[\text{PdF}_6]$ octahedra and is cubic ($Pa-3$). Further increase of pressure (40 GPa in PBEsol + U and 50 GPa in SCAN) leads to a structural transition into a polymorph consisting of 1D chains similar to those found in CuCl_2 -type polymorph (Fig. 5d). The symmetry of this collapsed chain polymorph corresponds to $Pnma$ space group. In the HSE06 picture, the contraction is less pronounced—down to 10% at 30 GPa, and the transition to the chain polymorph occurs via a different layered structure observed at 40 GPa, where the layers become more corrugated and more separated from each other (Fig. 5c). Ag atoms retain an approximately octahedral coordination, but the axial Cl contacts are now within the same layer as $[\text{AgCl}_4]$ squares. The elongation of octahedra due to Jahn–Teller effect is still noticeable (9%). Further compression to 50 GPa leads to a collapse to chains as in the other two methods. Changes in local coordination of Ag atoms in this polymorph are plotted in the bottom panel of Fig. 6.

The transitions described above can be seen as an abrupt drop in relative enthalpy in Fig. 2. In the previous contribution discussing relative stability of AgCl_2 candidate structures, AgF_2 -type emerged as the most likely candidate at higher pressures due to its comparatively low molar volume among the considered structures⁶. However, it appears that compression of AgF_2 -type produces a lot of strain in the structure, as evidenced by a strong increase of ΔH_f (Fig. 2), which is released through the aforementioned transition.

Arguably the most interesting pattern of pressure-induced transitions can be observed in the AuCl_2 -type nanotubular polymorph. The differences in outcomes of compression between the three computational approaches are the most pronounced for this system, although upon closer look we can identify their fundamental similarity. Recall that in the HSE06 approach, AuCl_2 -type is mixed-valent: Ag(I) species are connected to 3 Cl atoms in an approximately flat triangular pattern, while the Ag(III) sites appear as $[\text{AgCl}_4]$ square units, which are analogous to those in AgF_3 ¹². At 0 GPa, the triangular contacts average 2.53 Å, while the bonds in square units are 2.29 Å, which is even shorter than for Ag(II) in $[\text{AgCl}_4]$ square in CuCl_2 -type and AgF_2 -type polymorphs at the same pressure. This supports the assignment of the sites as Ag(I) and as Ag(III), respectively. Compression to 15 GPa induces a change in local coordination of the Ag(I) species, which picks up 4 Cl atoms along the axis perpendicular to the plane of the former triangle, resulting in a 4 + 3 coordination, with an average bond length of 2.61 Å. Meanwhile, the Ag(III) subunit retains a square coordination with a shorter average bond length of 2.27 Å. Further compression to 30 GPa leads to a rearrangement of nanotubes, which are now formed by a different combination of Ag and Cl atoms; importantly, all Ag atoms are coordinated by 4 Cl atoms in an approximately square-planar manner, with an average for the formerly Ag(III) sites at 2.33 Å and the formerly Ag(I) ones—2.38 Å. This convergence of the two sites in terms of local coordination points to a comproportionation process, whereby all Ag sites are now nominally Ag(II) species. The transition described above is shown in Fig. 7.

A very different scenario is observed in the SCAN picture (Fig. 8). At 0 GPa, the two Ag sites are already equivalent, but upon compression to 10 GPa, the local square-planar coordination of one of them is rotated by 90 degrees i.e., two of its four nearest Cl neighbors are substituted for another two, which leads to connections between nanotubes in the c direction. Further compression to 30 GPa results in an inward contraction of individual nanotubes. The local coordination of the Ag sites marked with red circle changes to more uniformly octahedral—a fifth Cl atom is picked up from a neighboring nanotube along the axis perpendicular to the $[\text{AgCl}_4]$ plane. The average length of the five Ag–Cl bonds for this Ag site is 2.51 Å (2.45–2.55 Å). The sixth nearest neighbor, on the opposite side of the former $[\text{AgCl}_4]$ is actually another Ag atom, located at a distance of 2.70 Å. (This connection is marked with a dashed line in Fig. 8.) Importantly, this new Ag...Ag contact is consistently shorter than the Ag–Ag distance in metallic silver at corresponding pressures (from SCAN calculations): 2.70 Å vs. 2.72 Å (30 GPa), 2.64 Å vs. 2.69 Å (40 GPa) and 2.60 Å vs. 2.67 Å (50 GPa). This leads us to infer a formation of a weak Ag–Ag interaction in this polymorph, which is a very interesting finding and reminiscent of a recent work, where a silver subchloride Ag_8Cl_6 was predicted, featuring $[\text{Ag}_6]$ subunits within its structure¹³. Further compression above 50 GPa leads to a substantial structural rearrangement: AgCl-like chains with square cross-section are formed, interspersed with Cl_2 molecules.

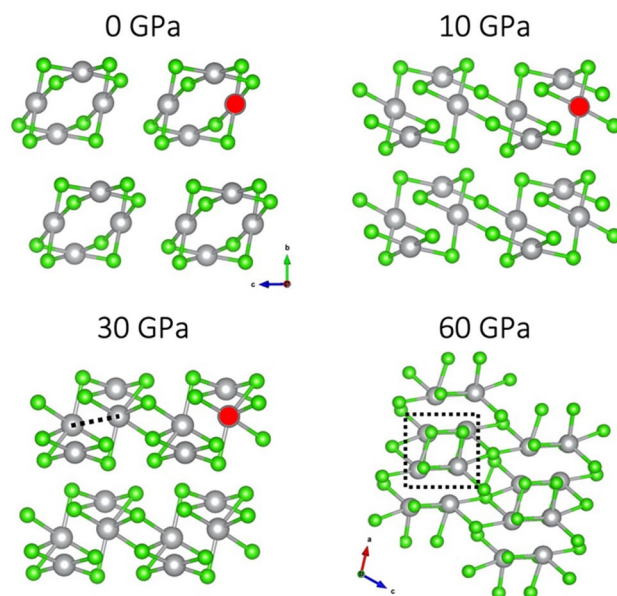


Figure 8. Structural transition of AuCl_2 -type polymorph in the SCAN picture. Nanotubes are viewed along the axis of propagation from 0 to 30 GPa. Note a different projection at 60 GPa, along the newly formed [AgCl] square nanowires. Red circles mark the Ag atom which experiences the pronounced changes in local coordination in the 0–30 GPa range.

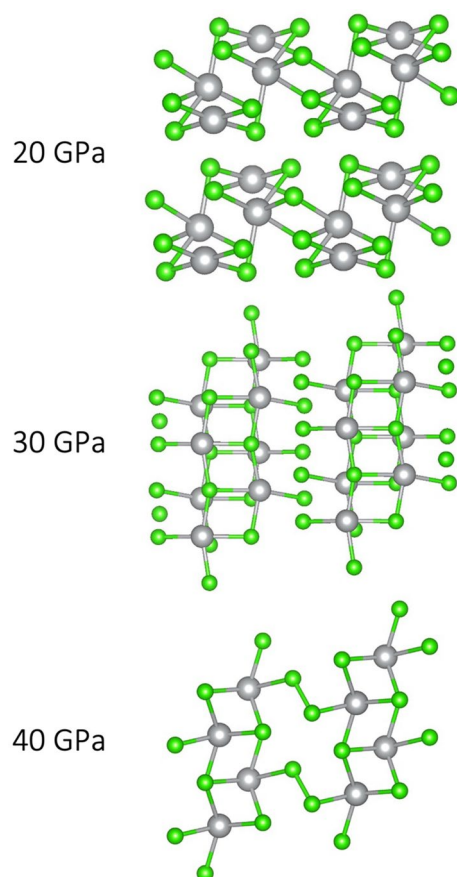


Figure 9. Structural transitions of AuCl_2 -type polymorph in the PBEsol + U picture.

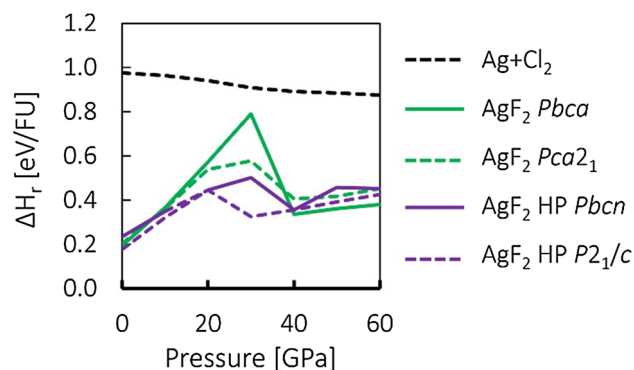


Figure 10. Comparison of ΔH_r pressure dependence for original (solid line) and phonon-relaxed (dashed line) structures of AgF_2 and HP- AgF_2 polymorphs of AgCl_2 .

A similar picture emerges from the PBEsol + U approach (Fig. 9). As in SCAN results, compression to 10 GPa leads to a rearrangement of local coordination of half of Ag sites. The subsequent contraction of nanotubes and formation of short Ag...Ag contacts is observed at a lower pressure of 20 GPa (compared to 30 GPa in SCAN). Upon further pressure increase to 30 GPa, a structure similar to Ag(I)r polymorph is formed, consisting of double layers of rocksalt-like AgCl interspersed with Cl atoms. The difference is that here, no discernible Cl–Cl molecules are formed—the distance between Cl atoms lying between AgCl layers is ca. 2.3 Å, compared to ca. 2.0 Å in solid molecular Cl_2 and in Ag(I)r polymorph. This is likely an artificial result, which will be further discussed in the “Electronic structure” section. Finally, compression to 40 GPa leads to rearrangement within AgCl layers, which increases the coordination number of Ag from 6 to 7 and the coordination environment resembles that in CsCl. Cl_2 molecules between the AgCl layers, characteristic of Ag(I)r polymorph, can also be discerned. Indeed, as can be seen in Fig. 2, this solution also converges with Ag(I)r polymorph in terms of ΔH_r .

As in the case of Ag(I)r solutions, formation of separate domains of AgCl and Cl_2 during structural transitions of AuCl_2 -type in PBEsol + U and SCAN picture, can be interpreted as another manifestation of the system’s tendency for $\text{AgCl} + \frac{1}{2}\text{Cl}_2$ phase separation, rather than as viable structural candidates. However, it should be pointed out that sodium and potassium chlorides with exotic stoichiometries as e.g. NaCl or Na_3Cl , have been predicted in the past^{14,15}.

Nanotubular AgF_2 -HP-type polymorph undergoes a structural collapse above 30 GPa in PBEsol + U results and above 60 GPa in SCAN results. The final structures do not resemble any of those discussed above; rather, they feature domains of connections between Ag and Cl atoms which do not form any extended and discernible pattern, and are instead interspersed with Cl_2 molecules. Since those solutions are consistently very high in relative enthalpy (ΔH_r), they will not be further analyzed here. (However, an example of the resulting structures can be found in Supplementary Information).

Dynamical stability of candidate AgCl_2 structures. In addition to the analysis of relative enthalpy of hypothetical polymorphs of AgCl_2 , we also investigated stability of their crystal structures by calculating (at the PBEsol + U level) phonon frequencies in Γ point of the first Brillouin zone, in the same unit cells as presented above. We found that the Ag(I)r and AuCl_2 types exhibit no imaginary phonon frequencies at Γ point in the studied range from 0 to 60 GPa. CuCl_2 -type polymorph exhibits two imaginary frequencies only at 0 GPa, which, when followed along their normal coordinates and relaxed, lead to the same structure as the original solution at 0 GPa (within 0.01 meV/FU in terms of total energy), so these may be considered as artifacts. We have, however, found structural instabilities in AgF_2 -type and nanotubular HP- AgF_2 -type, which we discuss below. Figure 10 compares pressure dependence of ΔH_r for the original (high symmetry) and phonon-relaxed (lower symmetry) structures in the two cases mentioned.

The layered AgF_2 -type polymorph is dynamically stable at 0 GPa, but at 10 GPa, an imaginary mode of B_{1u} symmetry emerges, which leads to a structure analogous to the previously reported non-centrosymmetric ($Pca2_1$), moderate-pressure polymorph of AgF_2 ⁴. This solution retains the layered arrangement, but the Ag atoms diverge from their position within the plane formed by surrounding Cl atoms (Fig. 11). The consequence of this transition is that the local coordination of Ag atoms changes from 4 + 2 (deformed octahedron) to 4 + 3 (Fig. 11), which likely minimizes repulsion between one of the lobes of the filled $d(z^2)$ orbitals and ligands. We proceeded to optimize this new solution in the same pressure range as the original AgF_2 (0–60 GPa, every 10 GPa). At 0 GPa, the original $Pbca$ remains more stable (by ca. 0.01 eV/FU in terms of ΔH_r). At 10 GPa, it becomes only slightly favored (by 0.004 eV/FU in terms of ΔH_r), and more favored at higher pressure up to 30 GPa. The $Pca2_1$ retains dynamic stability (no imaginary phonons in Γ) until 30 GPa. At higher pressure—like the original $Pbca$ solution—it collapses into a 1D structure, which is higher in energy than the previously discussed $Pnma$ structure resulting from the collapse of $Pbca$ (Fig. 10). The new collapsed structure features chains of AgCl interspersed with chains of Cl atoms along the c direction (the structure can be found in ESI).

Similarly, nanotubular HP- AgF_2 type exhibits an imaginary mode of B_{1g} symmetry already at 0 GPa. Following a normal coordinate of that mode and relaxing the structure, we obtain a lower-symmetry nanotubular structure

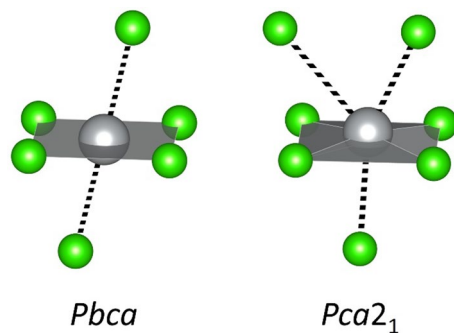


Figure 11. Comparison of local coordination of original and phonon-relaxed structures of AgF_2 -type at 10 GPa.

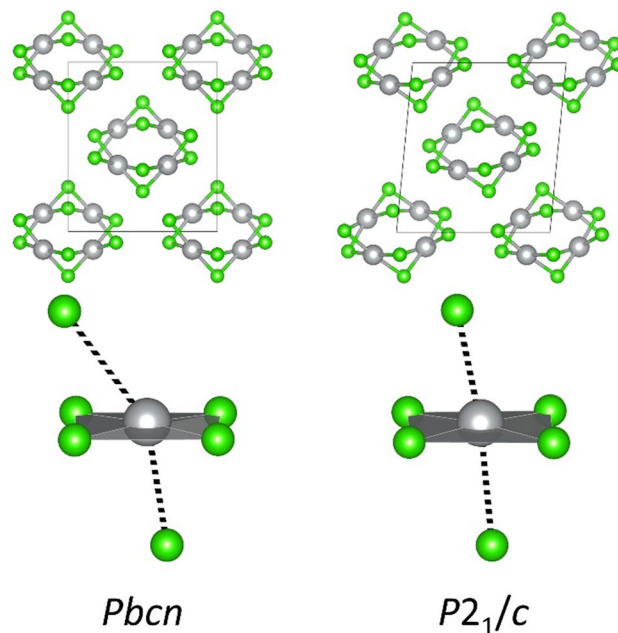


Figure 12. Comparison of structures and local coordination Ag atoms in original and phonon-relaxed structures of HP- AgF_2 -type at 0 GPa.

($P2_1/c$ space group), which is more stable than the original in terms of ΔH_f by 0.06 eV/FU already at 0 GPa. Likewise, we re-optimized this new phonon-relaxed solution in the 0–60 GPa range. The $P2_1/c$ solution remains more stable than the original $Pbcn$ in terms of ΔH_f , up until its own collapse above 20 GPa (a drop between 20 and 30 GPa can be seen for the purple dashed line in Fig. 10). It also remains dynamically stable (lack of imaginary phonons in Γ) within that range. Figure 12 presents the change in local coordination experienced by Ag atoms upon aforementioned relaxation at 0 GPa.

Importantly, for the Ag(I)r-type as well as CuCl_2 -type polymorphs at 0 GPa (i.e. the two most stable ones in terms of ΔH_f) we also calculated full phonon dispersion curves at the PBEsol + U level (in $2 \times 2 \times 2$ and $1 \times 2 \times 2$ supercells, respectively), which are shown in Supplementary Information. The results point to lack of imaginary phonons, which indicates metastability of these proposed structures. This leaves chance for the conceivable existence of these phases if prepared by some mildly exothermic reaction.

Electronic properties. As inferred from the previous paper⁶, antiferromagnetic superexchange in $\text{Ag}^{\text{II}}\text{Cl}_2$ can, in principle, be expected to be strong, since Ag–Cl bonding in this hypothetical compound would likely be more covalent in nature than in its AgF_2 counterpart. Of course, AgCl —the only currently known binary combination of silver and chlorine—is an ionic solid, as is AgF . However, previous studies of AgF_2 demonstrated a covalent character of Ag–F bonding in that compound, evidenced by X-ray photoelectron spectroscopy¹⁶ and by optical spectra¹⁷. In the former study, covalency increased in the sequence $\text{AgF} \rightarrow \text{AgF}_2 \rightarrow \text{AgF}_3$. Therefore, it is reasonable to expect a similar trend in AgCl_x compounds. On the other hand, Cl^- anions are larger and more diffuse and are therefore softer Lewis bases than F^- anions, which makes them more vulnerable to the strongly

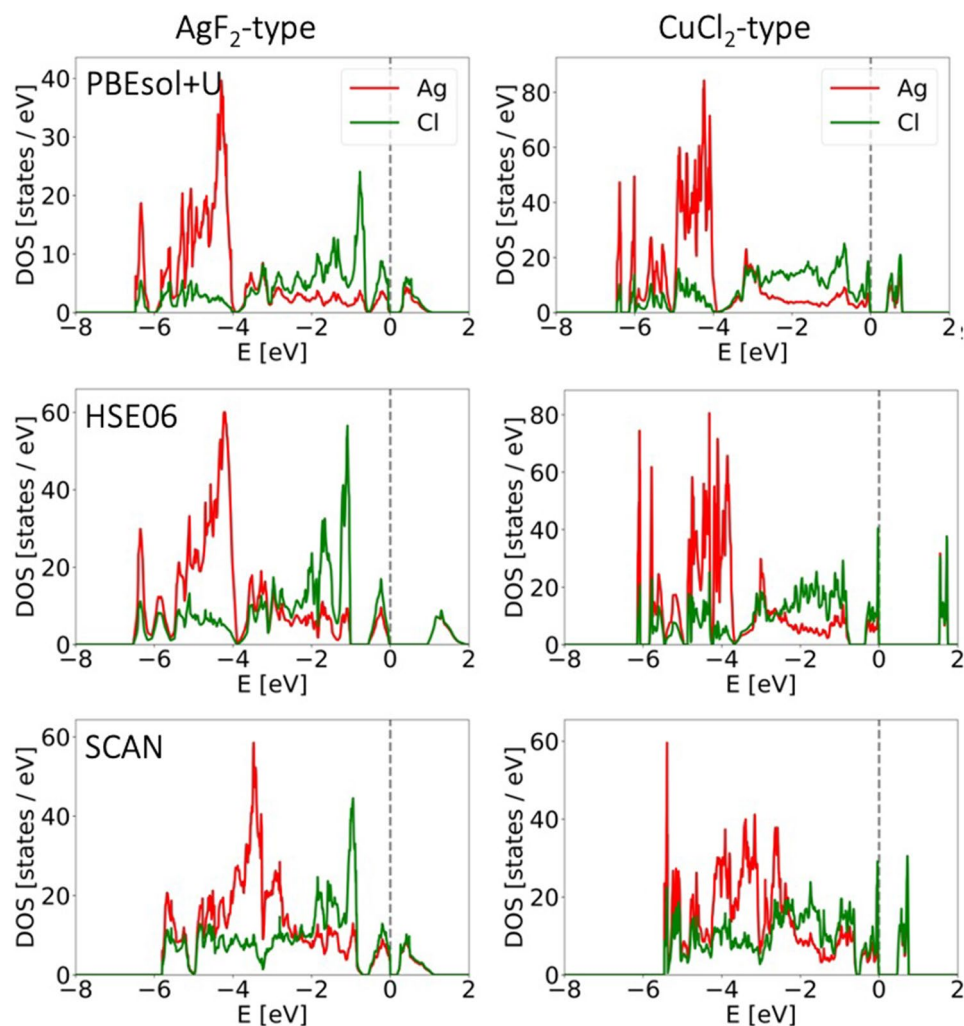


Figure 13. Comparison of eDOS plots for AgF_2 -type and CuCl_2 -type between different computational methods at 0 GPa.

oxidizing properties of Ag(II) cations. In addition, increasing pressure and the consequent reduction of interatomic distances increases orbital overlap, leading to broadening of electronic bands, which ultimately results in metallization of most known compounds (both ionic and covalent)⁷.

Electronic properties of the studied AgCl_2 candidate polymorphs were scrutinized in terms of (a) magnetic moments on Ag atoms and (b) fundamental band gap at the Fermi level in electronic density of states (eDOS) graphs. As it turns out, changes in the two parameters are strongly correlated in that the pressure at which the band gap closes coincides with disappearance of magnetic moment on Ag atoms.

An example of eDOS plots—for AgF_2 -type and CuCl_2 -type—at 0 GPa and comparison between the three computational methods is presented in Fig. 10. One noticeable feature is the composition of conduction band. In principle, AgCl_2 , just like the known AgF_2 , is expected to be a charge-transfer insulator, where the band gap arises between filled nonmetal states and empty metal states (upper Hubbard band, UHB)¹⁸. While this is certainly the case in AgCl_2 , we can see a substantial admixing of Cl states to the conduction band, with an almost perfect overlap and approximately equal contributions from Ag and Cl states. This indicates a strong covalence of the Ag–Cl bonds that is comparable or indeed even stronger than in AgF_2 ¹⁶. It should also be pointed out that “insulator” in this case refers to a non-zero band gap resulting from electronic correlation as per the aforementioned Zaanen-Sawatzky-Allen model¹⁸. Clearly, with a band gap in the range 0.2–1.5 eV (depending on the method) (Fig. 13), the two AgCl_2 polymorphs in question can be more accurately described as semiconductors.

Table 1 compares metallization pressure for selected polymorphs and between three methods. Metallization pressure is defined here as the lowest pressure point at which a solution exhibits null magnetic moments and null band gap. It can be seen that this value is the highest in HSE06 results. This coincides with the observation that the band gap is the largest for AgF_2 -type and CuCl_2 -type polymorphs in the HSE06 picture (Fig. 13). The differences between methods likely stem from the inclusion of exchange correlation in the hybrid-DFT-type functional, while in GGA-type PBEsol + U approach, electronic correlation, which is crucial for modelling open-subshell systems such as Ag(II) compounds, is only taken into account through U and J parameters (mentioned in “Methods”

	PBEsol + U	HSE06	SCAN
AgF ₂ -type	20 GPa	> 60 GPa ^a	10 GPa
CuCl ₂ -type	10 GPa	45 GPa	10 GPa
AgF ₂ HP-type	0 GPa	60 GPa	10 GPa
AuCl ₂ -type ^b	0 GPa	15 GPa ^c	10 GPa

Table 1. Pressure of metallization for different polymorphs of AgCl₂. ^aAlthough transformed into chains similar to CuCl₂-type, the polymorph retains residual magnetic moment and non-zero band gap at the maximal studied pressure of 60 GPa. Magnetic coupling is FM intra-chain and AFM inter-chain. ^bReopening of band gap occurs at higher pressures—see text. ^cThis polymorph is mixed-valent in HSE06 picture and is non-magnetic at 0 GPa.

section). HSE06 results can likely be considered the most accurate, since—in general—hybrid functionals like HSE06 are very well suited for predictions of band gaps in solids (compared to GGA and even meta-GGA)¹⁹.

The phase-separated Ag(I)r polymorph remains insulating within the studied pressure range and by account of all three methods. Structural transitions into phase-separated solutions observed for AuCl₂-type polymorph, which were discussed in the previous section, are also associated with reopening of the band gap. That is because constituent parts of these solutions—sublattices made up of ionic AgCl and of molecular Cl₂—are insulators. The fact that the solution for AuCl₂-type polymorph at 30 GPa in PBEsol + U picture retains metallic character after the aforementioned transition stems from the presence of dangling, unpaired Cl atoms on the outside of AgCl layers. Such arrangement should be unstable towards a Peierls distortion and formation of Cl₂ molecules, which is indeed what happens upon further compression to 40 GPa, and in SCAN picture. This testifies to the relatively poor suitability of PBEsol + U for describing electronic correlation.

Discussion

The Ag + Cl₂ phase diagram, which was studied here, consists of substances featuring a broad spectrum of chemical bonding types: metallic Ag, molecular Cl₂, ionic AgCl, as well as a variety of more or less covalently bonded polymorphs of AgCl₂, all of which have their own specific challenges when it comes to accurate theoretical description. Since AgCl₂ has not yet been observed experimentally, it is difficult to judge which of the three methods—GGA DFT (PBEsol + U), hybrid-DFT (HSE06) and meta-GGA DFT (SCAN)—is the most trustworthy for the assessment of stability of AgCl₂ at higher pressures—in particular, whether the region of stability seen in SCAN picture can be considered a reasonable finding. Our conclusions can to some extent be based on the results that these methods have provided when previously applied to other similar systems. To the best of our knowledge, a comparative computational study of an extended solid system comprised of a transition metal halide—like this one—has not been previously reported in literature. However, computations with hybrid functionals have been shown to provide excellent agreement with experimental data for e.g. ionic halides, where they are able to accurately reproduce lattice constants and bulk moduli of these solids²⁰. In general, hybrid functionals appear to have the potential to be the most accurate among DFT methods, superior to both GGA and meta-GGA²¹. Additionally, in the case of our system, HSE06 functional is the only one of the three methods which correctly reproduces the volume and intermolecular distances in solid Cl₂, which are determined by weak interactions between molecules.

Having said that, it is important to note that the overall picture which emerges from data presented here is remarkably consistent across the three computational methods, differing mostly in terms of pressure at which structural and electronic transitions are observed. Transitions of CuCl₂ and AgF₂ types reveal the tendency of the system to avoid repulsion between axial Cl atoms and filled d(z²) orbital of Ag atoms—through relative displacement of chains in the former and through transition from a layered 2D structure into 1D chains in the latter. A similar tendency is seen in pressure-induced phase transitions of AgF₂, where the high-pressure nanotubular structure can be viewed as a means both to maximize coordination number and to minimize the repulsion from the Ag d(z²) lone pair⁴. The transitions of AuCl₂-type and the relative stability of Ag(I)r polymorph firmly indicate that Ag^{II}Cl₂ is unstable towards charge transfer and phase separation into AgCl and Cl₂. Fundamentally, phase transitions observed in the studied polymorphs unfold upon pressure-induced decrease in distance between 1D or 2D structural constituents (chains, nanotubes, layers), which entails overcoming weak repulsive interactions between them. Among the three methods utilized here, the HSE06 functional, for reasons summarized above, is most likely best suited for description of those interactions.

Results reported in this work shed some light on properties and prospects of synthesis of the hypothetical AgCl₂. Most importantly, our study shows that high pressure does not stabilize the candidate polymorphs derived from the previous study—in particular, we see that the prediction of stability of AgF₂-type polymorph, which was based on a reasonable extrapolation from ambient-pressure data, nevertheless turned out not to be false⁶.

Of course, this work does not exhaust the list of possible candidates for the structure of AgCl₂. Although the studied candidates generally retain a positive enthalpy with respect to decomposition into AgCl + ½Cl₂, it is worth noting that the CuCl₂-type chain structure does not collapse into phase-separated polymorph even at 100 GPa in PBEsol + U and SCAN results. Analogous HSE06 calculations at 100 GPa were not performed, but based on the observation made here that transition pressures are reliably the highest within HSE06 approach, it is reasonable to predict that such collapse would not be seen in HSE06 picture at 100 GPa, either. The apparent lack of such transition pathway could mean that, in principle, obtaining it as a metastable phase could be possible

if e.g., elevated temperatures are used together with moderate pressures. Our previous results⁶, as well as earlier predictions by other authors^{22,23}, all consistently suggest that Ag^{II}Cl₂, if ever obtained, would likely be metastable.

Although the current study was focused on AgCl₂ stoichiometry only, the results of this study permit us to extrapolate observed trends towards the AgCl₃. The tendency of AgCl₂ stoichiometry to undergo decomposition to (AgCl)(Cl₂)_{1/2} may suggest that even at larger Cl contents, i.e. for AgCl₃ stoichiometry, one will observe phase separation to (AgCl)(Cl₂), or Ag⁺(Cl₃⁻)²⁴. A similar result is indicated by theoretical study for isolated AgCl₃ molecules in the gas phase²⁵.

Methods

Calculations were carried out using VASP software^{26–30}. Overall, three different computational methods were utilized (underlined are the names by which they are referred to throughout this work):

- I. PBEsol + U approach: GGA-type Perdew–Burke–Ernzerhof functional adapted for solids (PBEsol)³¹ was used, additionally taking into account Coulombic interactions between d electrons through U and J parameters³² explicitly set to 5 eV and 1 eV, respectively, and with correction for van der Waals interactions³³. Plane-wave cutoff energy was set to 800 eV. k-space sampling of ca. $2\pi \times 0.04 \text{ \AA}^{-1}$ was used for optimization and a denser k-spacing of ca. $2\pi \times 0.03 \text{ \AA}^{-1}$ was used for electronic density of states (eDOS) calculations. On an example structure of CuCl₂-type, this corresponds to $2 \times 7 \times 5$ and $3 \times 11 \times 7$ grid, respectively. Self-consistent-field convergence criterion was set to 10^{-7} eV. Additionally at this level, dynamical stability of resulting structures was assessed by calculating phonon frequencies at Gamma point of the Brillouin zone. Structures were further optimized to minimize forces acting on atoms to $\leq 10^{-5}$ eV/Å, and then Hessian matrix was constructed through finite differences approach as implemented in VASP. Phonon dispersion curves for selected systems were calculated and generated using PHONOPY interface^{34,35}. PBEsol + U is the cheapest among the three methods, but has been successfully utilized for prediction of high-pressure structures of Ag(II) compounds in the past^{2–4,36}.
- II. HSE06 approach: Hybrid-DFT HSE06 functional was utilized³⁷. Due to higher computational load of this method, a coarser k-space sampling of ca. $2\pi \times 0.05 \text{ \AA}^{-1}$ was used (e.g. $4 \times 4 \times 3$ grid in AgF₂-type) and plane-wave cut-off was set to 520 eV, with self-consistent-field convergence criterion of 10^{-7} eV. Although the cutoff energy is lower than in the other two methods, our convergence tests have shown that increasing it to e.g. 600 eV does not lead to a substantial improvement (i.e. the resulting total energy change is ca. 0.0001 eV/FU, which is of no practical consequence in our data). HSE06 is the most computationally demanding of the three methods, but provides the most accurate description of electronic properties¹⁹.
- III. SCAN approach: Meta-GGA-type, strongly constrained and appropriately normed (SCAN) functional was used³⁸, with correction for van der Waals interactions³⁹. Plane-wave cut-off energy was set to 800 eV and k-space sampling of ca. $2\pi \times 0.04 \text{ \AA}^{-1}$ was used, with self-consistent-field convergence criterion of 5×10^{-7} eV. A denser k-spacing of ca. $2\pi \times 0.03 \text{ \AA}^{-1}$ was used for eDOS calculations. SCAN approach is slightly more expensive than PBEsol + U, but still much cheaper than HSE06. This method has previously provided a value of antiferromagnetic coupling constant in AgF₂ that is in best agreement with experimental data².

The studied pressure range was 0 to 60 gigapascals (GPa), additionally extended to 100 GPa for SCAN calculations. Integration grids were not substantially increased in metallic solutions at higher pressures, but our convergence tests showed that an increase of grid density does not lead to a meaningful change in total energy (within 0.005 eV/FU) or in lattice constants after re-optimization (within 0.01 Å) at denser mesh. Pressure step was 10 GPa up to 60 GPa (or in some cases 15 GPa in HSE06 approach) and 20 GPa above 60 GPa. Cl₂ was considered in its solid polymorph with *Cmca* space group, which is known to be stable in the entire pressure range considered here⁴⁰. Similarly, metallic silver is also stable in its fcc structure within that range⁴¹. Known phase transitions of AgCl were taken into account when calculating relative enthalpy of AgCl₂ polymorphs⁴². A primitive unit cell of the KOH-type, high-pressure polymorph of AgCl was utilized in calculations, since it can be used to accurately describe the continuous nature of NaCl–KOH–TlI–CsCl sequence of phase transitions of AgCl^{42,43}.

Received: 27 August 2021; Accepted: 23 December 2021

Published online: 21 January 2022

References

1. Grochala, W. Silverland: The realm of compounds of divalent silver—and why they are interesting. *J. Supercond. Novel Magn.* **31**, 737–752 (2018).
2. Gawraczyński, J. *et al.* Silver route to cuprate analogs. *Proc. Natl. Acad. Sci.* **116**, 1495–1500 (2019).
3. Grzelak, A. *et al.* Metal fluoride nanotubes featuring square-planar building blocks in a high-pressure polymorph of AgF₂. *Dalton Trans.* **46**, 14742–14745 (2017).
4. Grzelak, A. *et al.* High-pressure behavior of silver fluorides up to 40 GPa. *Inorg. Chem.* **56**, 14651–14661 (2017).
5. Kurzydłowski, D., Derzsi, M., Zurek, E. & Grochala, W. Fluorides of silver under large compression. *Chem. Eur. J.* **27**, 5536–5545 (2021).
6. Derzsi, M., Grzelak, A., Kondratiuk, P., Tokár, K. & Grochala, W. Quest for compounds at the verge of charge transfer instabilities: The case of silver(II) chloride. *Curr. Comput.-Aided Drug Des.* **9**, 423 (2019).
7. Grochala, W., Hoffmann, R., Feng, J. & Ashcroft, N. W. The chemical imagination at work in very tight places. *Angew. Chem. Int. Ed.* **46**, 3620–3642 (2007).
8. Banks, M. G. *et al.* Magnetic ordering in the frustrated Heisenberg chain system cupric chloride CuCl₂. *Phys. Rev. B* **80**, 024404 (2009).

9. Dell'Amico, D. B., Calderazzo, F., Marchetti, F. & Merlino, S. Synthesis and molecular structure of $[\text{Au}_4\text{Cl}_8]$, and the isolation of $[\text{Pt}(\text{CO})\text{Cl}_3]^-$ in thionyl chloride. *J. Chem. Soc. Dalton Trans.* **1982**, 2257 (1982).
10. Kurzydłowski, D. *et al.* Local and cooperative Jahn-Teller effect and resultant magnetic properties of M_2AgF_4 ($\text{M} = \text{Na-Cs}$) phases. *Inorg. Chem.* **55**, 11479–11489 (2016).
11. Müller, B. G. Über Hochdruckmodifikationen von Palladiumfluorid und Silberfluorid. *Naturwissenschaften* **66**, 519–520 (1979).
12. Žemva, B. *et al.* Silver trifluoride: Preparation, crystal structure, some properties, and comparison with AuF_3 . *J. Am. Chem. Soc.* **113**, 4192–4198 (1991).
13. Derzsi, M., Uhliar, M. & Tokár, K. Ag_6Cl_4 : The first silver chloride with rare Ag_6 clusters from an ab initio study. *Chem. Commun.* **57**, 10186–10189 (2021).
14. Zhang, W. *et al.* Stability of numerous novel potassium chlorides at high pressure. *Sci. Rep.* **6**, 26265 (2016).
15. Zhang, W. *et al.* Unexpected stable stoichiometries of sodium chlorides. *Science* **342**, 1502–1505 (2013).
16. Grochala, W., Egdell, R. G., Edwards, P. P., Mazej, Z. & Žemva, B. On the covalency of silver-fluorine bonds in compounds of silver(I), silver(II) and silver(III). *ChemPhysChem* **4**, 997–1001 (2003).
17. Bachar, N. *et al.* Charge Transfer and dd Excitations in AgF_2 . arXiv preprint arXiv:2105.08862 (2021).
18. Zaanen, J., Sawatzky, G. A. & Allen, J. W. Band gaps and electronic structure of transition-metal compounds. *Phys. Rev. Lett.* **55**, 418–421 (1985).
19. Perdew, J. *et al.* Understanding band gaps of solids in generalized Kohn-Sham theory. *Proc. Natl. Acad. Sci.* **114**, 2801–2806 (2017).
20. Otero-de-la-Roza, A. & Johnson, E. R. Application of XDM to ionic solids: The importance of dispersion for bulk moduli and crystal geometries. *J. Chem. Phys.* **153**, 054121 (2020).
21. Price, A. J. A., Bryenton, K. R. & Johnson, E. R. Requirements for an accurate dispersion-corrected density functional. *J. Chem. Phys.* **154**, 230902 (2021).
22. Morris, D. F. C. The instability of some dihalides of copper and silver. *J. Phys. Chem. Solids* **7**, 214–217 (1958).
23. Rossini, F. D., Wagman, D. D., Evans, W. H., Levine, S. & Jaffe, I. Selected values of chemical thermodynamic properties. *Circ. Bureau Stand.* **500**, 272 (1952).
24. Haller, H. & Riedel, S. Recent discoveries of polyhalogen anions—From bromine to fluorine. *Z. Anorg. Allg. Chem.* **640**, 1281–1291 (2014).
25. Müller-Rösing, H. C., Schulz, A. & Hargittai, M. Structure and bonding in silver halides. A quantum chemical study of the monomers: Ag_2X , AgX , AgX_2 , and AgX_3 ($\text{X} = \text{F}, \text{Cl}, \text{Br}, \text{I}$). *J. Am. Chem. Soc.* **127**, 8133–8145 (2005).
26. Kresse, G. & Hafner, J. Ab initio molecular dynamics for liquid metals. *Phys. Rev. B* **47**, 558–561 (1993).
27. Kresse, G. & Hafner, J. Ab initio molecular-dynamics simulation of the liquid-metal-amorphous—Semiconductor transition in germanium. *Phys. Rev. B* **49**, 14251–14269 (1994).
28. Kresse, G. & Furthmüller, J. Efficiency of ab-initio total energy calculations for metals and semiconductors using a plane-wave basis set. *Comput. Mater. Sci.* **6**, 15–50 (1996).
29. Kresse, G. & Furthmüller, J. Efficient iterative schemes for ab initio total-energy calculations using a plane-wave basis set. *Phys. Rev. B Condens. Matter Mater. Phys.* **54**, 11169–11186 (1996).
30. Kresse, G. & Joubert, D. From ultrasoft pseudopotentials to the projector augmented-wave method. *Phys. Rev. B* **59**, 1758–1775 (1999).
31. Perdew, J. *et al.* Restoring the density-gradient expansion for exchange in solids and surfaces. *Phys. Rev. Lett.* **100**, 136406 (2008).
32. Liechtenstein, A. I., Anisimov, V. I. & Zaanen, J. Density-functional theory and strong interactions: Orbital ordering in Mott-Hubbard insulators. *Phys. Rev. B* **52**, R5467–R5470 (1995).
33. Grimme, S., Antony, J., Ehrlich, S. & Krieg, H. A consistent and accurate *ab initio* parametrization of density functional dispersion correction (DFT-D) for the 94 elements H–Pu. *J. Chem. Phys.* **132**, 154104 (2010).
34. Parlinski, K., Li, Z. Q. & Kawazoe, Y. First-principles determination of the soft mode in cubic ZrO_2 . *Phys. Rev. Lett.* **78**, 4063–4066 (1997).
35. Togo, A. & Tanaka, I. First principles phonon calculations in materials science. *Scripta Mater.* **108**, 1–5 (2015).
36. Grzelak, A. *et al.* Persistence of mixed and non-intermediate valence in the high-pressure structure of silver(I, III) oxide, AgO : A combined Raman, X-ray diffraction (XRD), and density functional theory (DFT) study. *Inorg. Chem.* **56**, 5804–5812 (2017).
37. Krukau, A. V., Vydrov, O. A., Izmaylov, A. F. & Scuseria, G. E. Influence of the exchange screening parameter on the performance of screened hybrid functionals. *J. Chem. Phys.* **125**, 224106 (2006).
38. Sun, J., Ruzsinszky, A. & Perdew, J. P. Strongly constrained and appropriately normed semilocal density functional. *Phys. Rev. Lett.* **115**, 036402 (2015).
39. Peng, H., Yang, Z.-H., Perdew, J. P. & Sun, J. Versatile van der Waals density functional based on a meta-generalized gradient approximation. *Phys. Rev. X* **6**, 041005 (2016).
40. Dalladay-Simpson, P. *et al.* Band gap closure, incommensurability and molecular dissociation of dense chlorine. *Nat. Commun.* **10**, 1134 (2019).
41. Dewaele, A., Torrent, M., Loubeyre, P. & Mezouar, M. Compression curves of transition metals in the Mbar range: Experiments and projector augmented-wave calculations. *Phys. Rev. B* **78**, 104102 (2008).
42. Hull, S. & Keen, D. Pressure-induced phase transitions in AgCl , AgBr , and AgI . *Phys. Rev. B* **59**, 750–761 (1999).
43. Catti, M. & di Piazza, L. Phase equilibria and transition mechanisms in high-pressure AgCl by Ab initio methods. *J. Phys. Chem. B* **110**, 1576–1580 (2006).

Acknowledgements

A.G. would like to thank Dr. Mariana Derzsi for fruitful discussions and comments at the initial stage of this work's development. A.G. acknowledges the contribution from the Polish National Science Center (NCN)—Preludium project no. 2017/25/N/ST5/01976. This research was carried out with the support of the ICM computer center, University of Warsaw under grant SAPPHERE (no. GA83-34 and G85-892).

Author contributions

A.G. and W.G. conceived the study. A.G. performed computations, analyzed the results, made the figures and wrote the manuscript. W.G. reviewed the manuscript.

Competing interests

The authors declare no competing interests.

Additional information

Supplementary Information The online version contains supplementary material available at <https://doi.org/10.1038/s41598-022-05211-0>.

Correspondence and requests for materials should be addressed to A.G.

Reprints and permissions information is available at www.nature.com/reprints.

Publisher's note Springer Nature remains neutral with regard to jurisdictional claims in published maps and institutional affiliations.



Open Access This article is licensed under a Creative Commons Attribution 4.0 International License, which permits use, sharing, adaptation, distribution and reproduction in any medium or format, as long as you give appropriate credit to the original author(s) and the source, provide a link to the Creative Commons licence, and indicate if changes were made. The images or other third party material in this article are included in the article's Creative Commons licence, unless indicated otherwise in a credit line to the material. If material is not included in the article's Creative Commons licence and your intended use is not permitted by statutory regulation or exceeds the permitted use, you will need to obtain permission directly from the copyright holder. To view a copy of this licence, visit <http://creativecommons.org/licenses/by/4.0/>.

© The Author(s) 2022